J. Fluid Mech. (1971), *vol.* 46, *part* 3, *pp.* 477–500
Printed in Great Britain

Measurements of subsonic jet noise and comparison with theory

By P. A. LUSH

Institute of Sound and Vibration Research,
University of Southampton

(Received 31 July 1970)

Measurements of the noise field from a 25 mm diameter subsonic air jet are presented. These results are analysed in some detail by determining both the jet velocity dependence and the directivity of the intensity of the radiation in $\frac{1}{3}$-octave bands at particular values of the frequency parameter,

$$(fD/V_J)(1-M_c\cos\theta).$$

This procedure should ensure that a particular source in a geometrically similar position in the jet is always observed, whatever the jet velocity, diameter and emission angle.

These results are compared with the predictions of Lighthill's (1952) theory of convected quadrupoles. It is shown that the theory predicts the variation of the intensity with jet velocity and emission angle provided that the observed frequency is below a certain critical value, which depends on jet diameter and emission angle and is independent of jet velocity. Above this critical frequency, the predicted variations overestimate the measurements and it appears that the convective amplification predicted by the theory is much reduced. The variation of this critical frequency is explained by assuming that substantial interaction occurs between the radiated sound and the jet flow when the wavelength of the sound becomes shorter than the sound path length in the jet flow.

1. Introduction

A series of measurements of the noise field from a 25 mm diameter subsonic jet has been carried out in order to investigate the characteristics of the noise in some detail. Considerable care has been taken to ensure that unwanted noise sources, such as valves and ducting upstream of the nozzle, are insignificant compared with the jet mixing noise. The dependence on jet velocity, the directivity and the spectra have been measured and compared in detail with the predictions of Lighthill's (1952) theory of convected quadrupoles. The comparison is done first for the intensity over all frequencies as a function of jet velocity and emission angle to the jet axis.

More detail of the noise characteristics is sought by extending this analysis to the velocity dependence and directivity of the intensity in particular $\frac{1}{3}$-octave frequency bands. To obtain meaningful results it is necessary to correct

the observed frequency for variations in jet velocity, and, if results from several nozzle sizes are being compared, in jet diameter. The velocity dependence and directivity are therefore examined at a constant Strouhal number rather than a constant frequency. This procedure should ensure that the sources in geometrically similar positions are analysed whatever the jet velocity and diameter. To conform with the model of convected sources, the observed frequency is also Doppler-corrected so that the same source frequency is examined in each case, whatever the convection velocity and emission angle.

Using this method, the theoretically predicted velocity dependence and directivity can be checked at several frequencies across the spectrum. In addition, on assuming that the noise field is axisymmetric, an estimate of the overall power and the power in various $\frac{1}{3}$-octave bands can be made, and these can also be checked with the predictions. In this way it is hoped to build up a detailed picture of the accuracy of Lighthill's theory as it has been commonly applied to jet noise estimation.

2. The jet noise rig

The jet noise rig consists essentially of a nozzle exhausting into a large anechoic chamber which measures $9 \times 9 \times 7{\cdot}2$ m. The chamber is lined on all walls inside with acoustic foam wedges, 1 m long, which render it anechoic down to about 100 Hz. Compressed air at approximately room temperature is supplied to the nozzle via a control valve and a silencer settling chamber. This chamber is cylindrical with a diameter of 300 mm and a length of 1·5 m and is designed to reduce the valve noise so that it is negligible compared with the jet mixing noise. This is achieved by lining the chamber with acoustic foam, 50 mm thick, and by placing four baffles in the chamber at intervals of 300 mm. The baffles overlap so that there is no direct sound path. The valve noise can just be detected with the nozzle removed. It consists of tones at about 5, 8 and 12 kHz of intensity 30–45 dB.† This level is always below the jet mixing noise.

The resulting settling chamber has a diameter of 150 mm, which gives an area contraction ratio of 36:1 when used with a 25 mm diameter convergent nozzle. The large contraction ratio ensures that the flow velocity in the settling chamber is very low, rising to a maximum of about 5 m/s at choking. This, in turn, ensures that the noise generated by the flow in the duct is very small.

The nozzle is made of fibreglass and specially contoured to give a uniform velocity profile at the exit. It has an exit diameter of 25 mm and two extension pieces can be fitted to further reduce the exit diameter to 12·5 and 6·25 mm. A separate nozzle with an exit diameter of 50 mm can also be used.

The microphone may be mounted at various angles to the jet axis using a permanent stand constructed of light steel framework. The stand resembles the quadrant of a circle of radius 3 m and, since the jet issues vertically downwards from the roof of the chamber, it is mounted vertically with the centre of the quadrant at the nozzle exit. Microphone holders are positioned along the stand at intervals of $7\frac{1}{2}°$ from $7\frac{1}{2}°$ to 105° to the jet axis (figure 1).

† Acoustic intensities are quoted throughout in dB relative to 10^{-12} W/m^2.

The measuring and recording equipment consists of a 13 mm Bruel and Kjaer condenser microphone (microphone cartridge type 4133 and cathode follower type 2615), which is used in conjunction with a B & K microphone amplifier (type 2603), bandpass filter set (type 1612), and level recorder (type 2305).

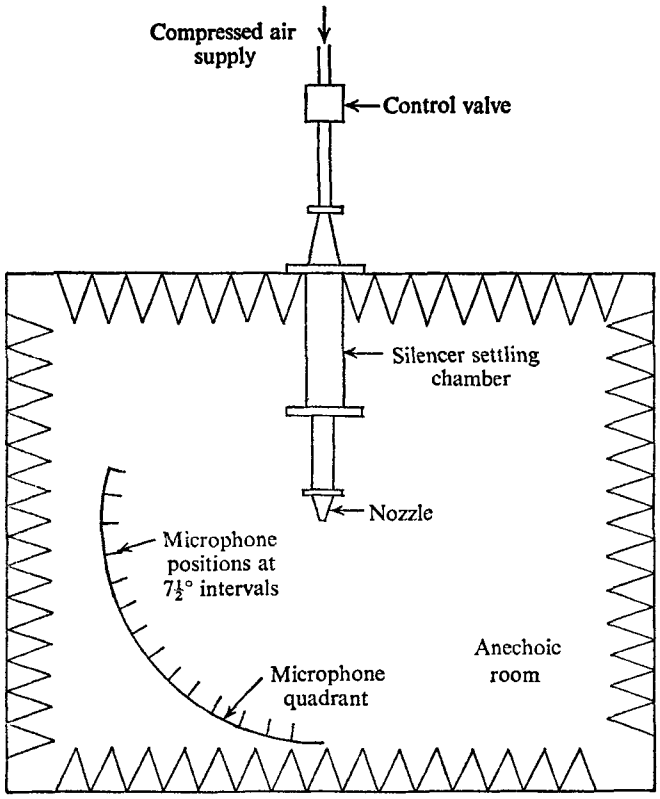

FIGURE 1. Schematic layout of jet noise rig.

3. Measurement details

Measurements of $\frac{1}{3}$-octave sound pressure level spectra, between frequencies of 20 Hz and 40 kHz, have been made at all angles to the jet axis between $7\frac{1}{2}°$ and 105° at intervals of $7\frac{1}{2}°$. For each angular position the jet velocity was varied in about ten steps from 75 to 300 m/s. The maximum jet velocity corresponded to nozzle choking. These measurements were obtained mainly for the 25 mm nozzle, although a limited set of measurements were also taken for nozzles of 50, 12·5, and 6·25 mm diameter. For these experiments the stagnation temperature in the settling chamber was assumed to be equal to the room temperature after several hours of running. In addition the atmospheric pressure was measured at regular intervals during testing and frequent checks were made on the microphone calibration using a B & K pistonphone (type 4220).

Satisfactory measurements could not be obtained below about 90 m/s for the 25 mm jet because the jet noise was merging into the background noise at

low frequencies around 100 Hz. The background noise in the anechoic chamber was about 50 dB overall. At higher jet velocities the low-frequency noise increased but not as rapidly as the jet noise. It appears that, at these low frequencies, the microphone was still in the near field of part of the jet. Measurements at these frequencies for jets of different sizes show that the intensity falls off rapidly with decrease in size or equivalently with increase in microphone distance, whereas the jet noise decreases, as expected, at 6 dB for every doubling of the distance. This near field noise sets a low-frequency limit on the analysis of the far-field jet noise at around 100 Hz for the 25 mm jet (figure 2).

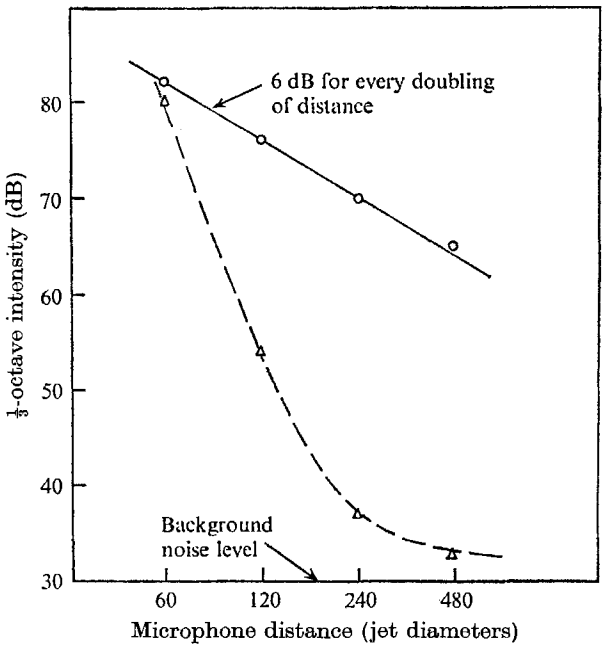

FIGURE 2. Decay of jet noise with distance at 15° to the axis.
△, low-frequency (near field); ○, peak frequency (far field).

At the other end of the jet velocity range, the appearance of shock cell tones at about 10 kHz, when the nozzle becomes choked, sets an upper speed limit. The microphone response becomes non-linear above about 10 kHz, and measurements above this frequency will be in error, since no microphone or atmospheric absorption corrections have been applied. However, this is not important since the frequencies of interest for the 25 mm jet are below 10 kHz. When the microphone was placed at $7\frac{1}{2}°$ to the jet axis, a nose cone was fitted because the microphone was in the outer edge of the jet. Although the signal was dominated by the jet pressure fluctuations, part of the noise spectrum could be observed.

It is possible that errors in measurements have occurred because of reflexions of the noise from the microphone stand and supporting structure. Efforts were made to minimize this by covering the stand with acoustic foam 50 mm thick. During preliminary testing a substantial ground-reflexion ripple was noticed in the spectra at low frequencies. This was eliminated by removing part of the

supporting structure. No other reflexion effects were discovered but the possibility of their presence should be borne in mind when interpreting results. It is felt that the checks done on the different size nozzles should help to distinguish between actual changes in the noise characteristics and those caused by faults in the measurement technique. In fact it was found that there were no major unexplained differences between the results from any of the nozzles tested.

4. Development of theory for comparison with results

Lighthill's (1952) result for the far-field intensity of the noise generated by a turbulent flow forms the starting-point for this analysis. This result was modified slightly to apply to the noise radiation from a jet by Ffowcs Williams (1963) (see also Lighthill 1963).

The result for the far-field intensity, I, may be written in dimensional form as follows:

$$I \sim \frac{\rho_m^2 V_J^8 D^2}{\rho_0 a_0^5 R^2} \frac{D(\theta)}{(1-M_c\cos\theta)^5}, \tag{1}$$

where ρ_m is the density in the mixing region, V_J the jet velocity, D the nozzle diameter, ρ_0 and a_0 the density and speed of sound in the external fluid, R the distance from the jet to the observer and θ the angle between the direction of emission of sound and the downstream jet axis. The function $D(\theta)$ is the directivity of the unconvected quadrupole distribution and M_c is the speed of convection of the quadrupoles divided by the speed of sound in the external fluid.

Ffowcs Williams (1963) showed that the factor $(1-M_c\cos\theta)^{-5}$ should be modified to $\{(1-M_c\cos\theta)^2+\alpha^2M_c^2\}^{-\frac{5}{2}}$ when the convection Mach number approaches unity. For the analysis in this paper the convection velocity is taken to be 0·65 of the jet velocity, a result given by Davies, Fisher & Barratt (1963). In the experiments reported here the maximum jet velocity is about 300 m/s, thus convection Mach numbers do not exceed about 0·6. Taking the value of α equal to 0·3, as given by Davies *et al.* (1963), it may be shown that the maximum error in the directivity factor caused by ignoring the $\alpha^2M_c^2$ factor is 1 dB at $M_c = 0{\cdot}5$. Similarly, it may be shown that the error in the Doppler factor is about 5 %. Consequently, the factor $\alpha^2M_c^2$ is neglected in the following analysis.

In addition, since the stagnation temperature of the jet in these experiments is equal to the ambient temperature, the density in the jet core will be only 20 % greater than the ambient density at the highest jet velocity tested. Thus, the density in the mixing region is taken to be equal to the ambient density. It may be shown that, at the maximum jet velocity tested, the error involved is less than 1 dB.

The sound power may be obtained from the intensity by assuming that the sound field is axisymmetric and integrating over a sphere of radius R centred on the nozzle exit. The sound power, P, is then related to the intensity, I, by

$$P = 2\pi R^2 \int_0^\pi I(\theta)\sin\theta\, d\theta. \tag{2}$$

It is now assumed that there are no preferred orientations of quadrupoles so that $D(\theta)$ is unity in (1). This assumption may be justified for the overall intensity on examining the experimental measurements, which show that at low jet velocities, where convection effects are small, the directivity is almost uniform.

On substituting for I in (2) it may be shown that the sound power is given dimensionally by (Lighthill 1962)

$$P \sim \frac{\rho_0 V_J^8 D^2}{a_0^5} \frac{1+M_c^2}{(1-M_c^2)^4}, \tag{3}$$

where the density in the mixing region has been replaced by the ambient density, ρ_0.

For a more detailed analysis of the noise characteristics, it is necessary to study the spectral density of the sound field. An expression for the spectral density of the intensity, $W(f)$, has been derived by Ffowcs Williams (1963) and it may be written in dimensional form as follows:

$$W(f) \sim (D^3/\rho_0 a_0^5 R^2) f^4 H(f_s) D(\theta), \tag{4}$$

where f is the observed frequency and f_s is the frequency observed in a frame of reference convected at Mach number M_c, and is related to the observed frequency by the Doppler factor,

$$f_s = f(1 - M_c \cos\theta). \tag{5}$$

The function $H(f_s)$ is the Fourier transform of the correlation function of Lighthill's stress tensor, $T_{ij} = \rho u_i u_j + p_{ij} - a_0^2 \rho \delta_{ij}$ (Lighthill 1952). It is related dimensionally to T_{ij} by $H(f_s) \sim \overline{T^2} D^3 f_s^{-1}$. The quantity $H(f_s)$ is also a function of the wave-number of the turbulence, but, since effects associated with near-sonic convection are neglected here, it is appropriate to omit this term from the argument of H.

Since the sound is measured in proportional bands in these experiments, the spectral density must be weighted by the frequency to give a quantity proportional to the intensity in a $\frac{1}{3}$-octave band. On multiplying (4) by f, and using (5), the intensity of sound in a $\frac{1}{3}$-octave band is given by

$$\{W(f)f\} \sim \frac{D^3}{\rho_0 a_0^5 R^2} \frac{f^4 \{H(f_s) f_s\} D(\theta)}{1 - M_c \cos\theta}, \tag{6}$$

where the quantities in curly brackets may be interpreted as $\frac{1}{3}$-octave spectra.

The observed frequency, f, is now eliminated from the right-hand side by using (5), and the quantities f_s and $\{H(f_s)f_s\}$ are expressed in their non-dimensional forms,

$$f_s D/V_J \quad \text{and} \quad \{H(f_s)f_s\}/\rho_0^2 V_J^4 D^3.$$

The expression for the $\frac{1}{3}$-octave intensity becomes

$$\{W(f)f\} \sim \frac{\rho_0 V_J^8 D^2}{a_0^5 R^2} \left[\frac{f_s D}{V_J}\right]^4 \frac{\{H(f_s)f_s\}}{\rho_0^2 V_J^4 D^3} \frac{D(\theta)}{(1 - M_c \cos\theta)^5}. \tag{7}$$

If the quantity $f_s D/V_J$ is kept constant, the non-dimensional spectrum function involving $H(f_s)$ is also constant, and the expression reduces to

$$\{W(f)f\} \sim \frac{\rho_0 V_J^8 D^2}{a_0^5 R^2} \frac{D(\theta)}{(1 - M_c \cos\theta)^5}. \tag{8}$$

Thus, if the $\frac{1}{3}$-octave results are analysed so that

$$f_s D/V_J = (fD/V_J)(1 - M_c \cos\theta) = \text{const.}, \tag{9}$$

then the $\frac{1}{3}$-octave intensities will be independent of frequency and will show a velocity dependence given by $V_J^8(1 - M_c \cos\theta)^{-5}$ and a directivity given by $D(\theta)(1 - M_c \cos\theta)^{-5}$. It should be noted that any preferred orientations of the quadrupoles contained in the factor $D(\theta)$ do not affect the velocity dependences at a given emission angle.

The condition imposed by (9) may be interpreted physically by imagining that the observed frequency is first corrected for Doppler shift to convert to the source frequency and then the Strouhal number correction ensures that the intensity is measured at the same point on the spectrum relative to the peak. In this way it is ensured that the source in a geometrically similar position in the jet is observed, whatever the emission angle, jet diameter and jet velocity.

A similar analysis may be carried out for the acoustic power. The power in a $\frac{1}{3}$-octave band at frequency f may be calculated by integrating the intensity $\{W(f)f\}$, given by (6), over all angles using (2), to obtain

$$\{P(f)f\} = 2\pi R^2 \int_0^\pi \{W(f)f\} \sin\theta \, d\theta, \tag{10}$$

where $P(f)$ is the spectral density of the acoustic power and $\{P(f)f\}$ is the acoustic power in a $\frac{1}{3}$-octave band. In order to isolate the power radiated from a particular source fluctuating at frequency f_s, the observed frequency, f, must be corrected by the Doppler factor according to (5). To ensure that the source observed is in a geometrically similar position in the jet irrespective of the jet velocity and diameter, the source frequency must be expressed as a Strouhal number and (9) satisfied. Thus, the integration of (10) should be applied to (7) with $f_s D/V_J$ kept constant. In this case, both $f_s D/V_J$ and $H(f_s)$ are independent of emission angle and for simplicity it is assumed that all the quadrupoles are randomly oriented so that $D(\theta)$ is unity. Hence it may be shown that the power in a $\frac{1}{3}$-octave band at frequency f is given by

$$\{P(f)f\} \sim \frac{\rho_0 V_J^8 D^2}{a_0^5} \frac{1 + M_c^2}{(1 - M_c^2)^4}. \tag{11}$$

This result shows that at any frequency $f_s D/V_J$ the velocity dependence of the power in a $\frac{1}{3}$-octave band is given by

$$V_J^8 (1 + M_c^2)/(1 - M_c^2)^4.$$

In the subsequent analysis of the experimental results, the frequency parameter, $f_s D/V_J$, given by (9), is put equal to four typical values, namely, 0·03, 0·10, 0·30 and 1·0. The values of the intensity in a $\frac{1}{3}$-octave band, $\{W(f)f\}$, are then displayed as functions of jet velocity, V_J, and emission angle, θ, for each value of the frequency parameter. These results are then compared directly with the predictions of (8), assuming that all the quadrupoles are randomly oriented so that $D(\theta)$ is unity. Similarly, the acoustic power in a $\frac{1}{3}$-octave band is calculated by rewriting (10) as follows,

$$\{P(f)f\} = 2\pi R^2 \Delta\theta \, \Sigma \{W(f)f\} \sin\theta. \tag{12}$$

Thus the intensities, $\{W(f)f\}$, expressed in W/m^2 and not decibels, at each emission angle are weighted with $\sin\theta$ and summed over all angles. The power in watts is obtained by multiplying by the constant $2\pi R^2\Delta\theta$. There will be an error in these calculations because the intensity is not measured close to the jet axis and between 105° and 180° to the axis. However, the error will probably not be serious since the intensities close to the axis are rendered less important by the $\sin\theta$ weighting and the intensities in the arc 105–180° are well below the peak intensity. It should be noted that the quantity $\{P(f)f\}$ could not be obtained by direct measurement since the frequency, f, changes with emission angle, θ, because of the Doppler effect. These results are displayed as a function of jet velocity for each value of the frequency parameter, and compared directly with the prediction of (11).

No attempt is being made, in this work, to use the theory to predict the absolute level of radiation. Whenever theoretical and experimental curves are compared the absolute level of the theory is adjusted for the best fit with the data. Conversely, there is no opportunity to adjust the velocity scale since the convection velocity has been arbitrarily fixed at 0·65 of the jet velocity.

5. The principal results

The measurements of overall intensity are compared with the predictions of the theory (equation (1)). In comparing the overall intensities it is justifiable to assume that all the quadrupoles are randomly oriented so that $D(\theta)$ is unity. A typical set of these measurements for the 25 mm nozzle with the appropriate theoretical curves are shown in figures 3 and 4. These measurements were found to be repeatable to within ± 1 dB. The main feature of these results (figure 3) is that the intensity at 90° to the jet axis varies as near the eighth power of jet velocity, from about 90 m/s to 300 m/s, as predicted by the theory. A more accurate measurement of the jet velocity power, which also includes the density correction factor, shows that this power is actually 7·5. The increase in intensity at the highest velocities is due to shock cell tones which dominate the broadband noise. At other angles to the jet axis, the measured intensity falls below the prediction at the upper end of the speed range, and the velocity dependences are again near the eighth power. The theoretical curves at 15° and 45° on this figure have not been adjusted vertically relative to that at 90° and hence have the correct amount of convective amplification above the 90° line.

The directivities shown in figure 4 indicate that the intensity is directional with a peak more or less along the jet axis. As the jet velocity is increased, the directivity becomes more marked and at the highest velocity the peak is at $22\frac{1}{2}$° and the amplification from 90° to the peak angle is about 10 dB. However, the amount of amplification is overestimated by the theory, particularly at the higher speeds. Nevertheless, it appears that the directivity is qualitatively related to the convective amplification of the theory and, as mentioned earlier, at the low jet velocities the directivity is almost uniform, indicating the absence of any predominant quadrupole orientation for the overall intensity. In this figure, the theoretical directivities have been adjusted vertically for the best fit.

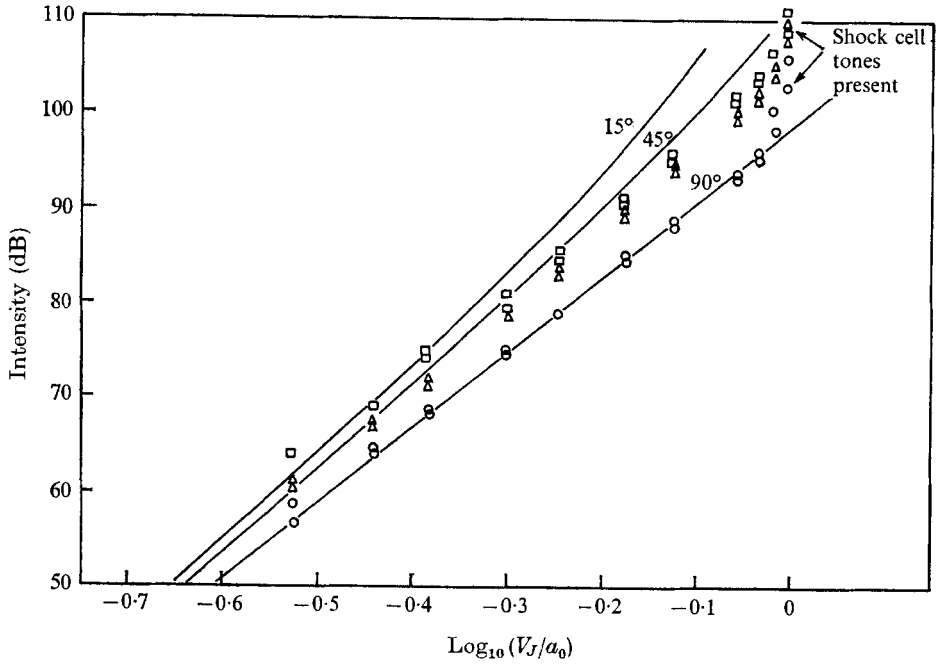

FIGURE 3. Velocity dependence of intensity compared with theory. □, 15°; △, 45°; ○, 90°; ——, theory, equation (1).

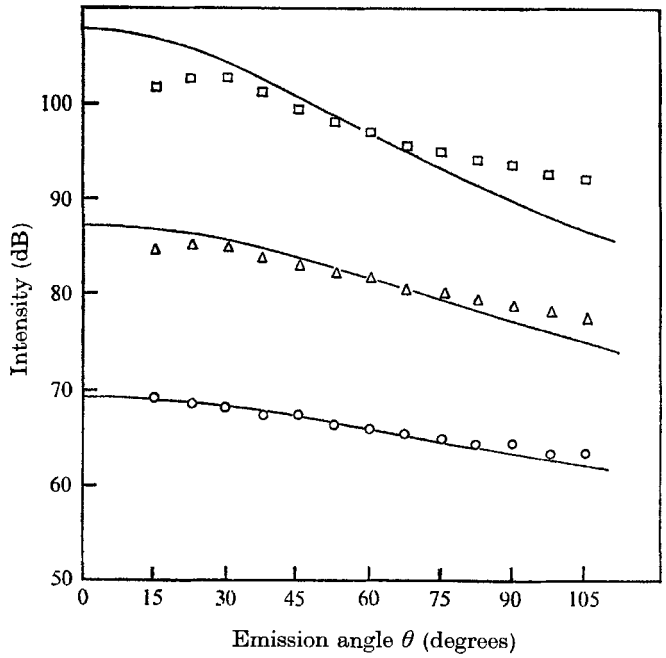

FIGURE 4. Directivities compared with theory. Jet velocities: ○, 125 m/s; △, 195 m/s; □, 300 m/s; ——, theory, equation (1).

The acoustic power† may be obtained by using an equation similar to (12), which relates the overall power to the overall intensity. When this is done the results are plotted as a velocity dependence as shown in figure 5. This figure also shows the results from the 12·5 mm nozzle corrected by (3) to a nozzle diameter of 25 mm. It can be seen that the variation of power of both jets is in agreement and the velocity dependence is near the eighth power. The theoretical line derived from (3) increases more rapidly with velocity than do the measurements.

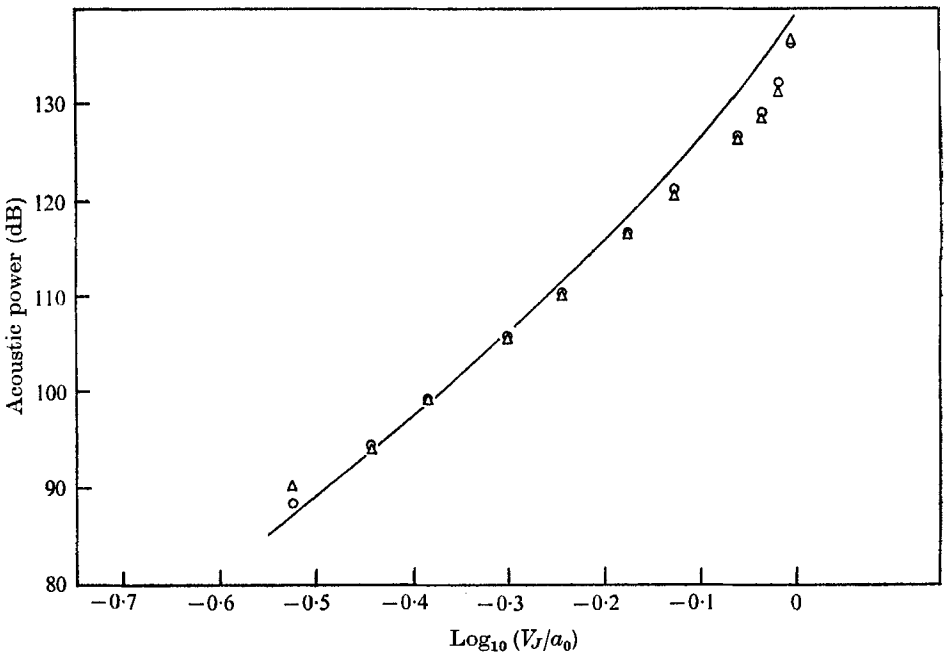

FIGURE 5. Velocity dependence of acoustic power compared with theory. ○, 25 mm jet; △, 12·5 mm jet; ——, theory, equation (3).

The value of the constant of proportionality of (3) without the convective amplification factor can be calculated from these results. It is found to lie between 3 and 4×10^{-5}. The acoustic efficiency based on the jet energy flux is therefore $0{\cdot}8\text{–}1{\cdot}0 \times 10^{-4}(V_J/a_0)^5$.

Typical $\frac{1}{3}$-octave spectra, as taken straight from the level recorder, are shown in figures 6–8. It can be seen that the spectrum shape changes rapidly with emission angle (figure 6). At 90° to the jet axis (figure 8) the spectrum is broad and fairly smooth with a peak frequency, scaling as a Strouhal number, in the region of $0{\cdot}8V_J/D$. The growth of the spectrum at low frequencies is about 6–9 dB per octave and the decay at high frequencies is about 2–3 dB per octave. This is in agreement with the results of dimensional arguments which associate low frequencies with the fully developed jet and high frequencies with the mixing region (Lighthill 1963).

† Acoustic power is quoted throughout in dB relative to 10^{-13} W.

However, at 15° to the jet axis (figure 7) the spectrum shape changes and the peak becomes more marked and shifts to a lower frequency. Moreover, the peak frequency does not scale as a Strouhal number and remains almost constant at 2000 Hz over the whole velocity range. The growth of the spectrum at low frequencies is again about 9 dB per octave, in agreement with theoretical

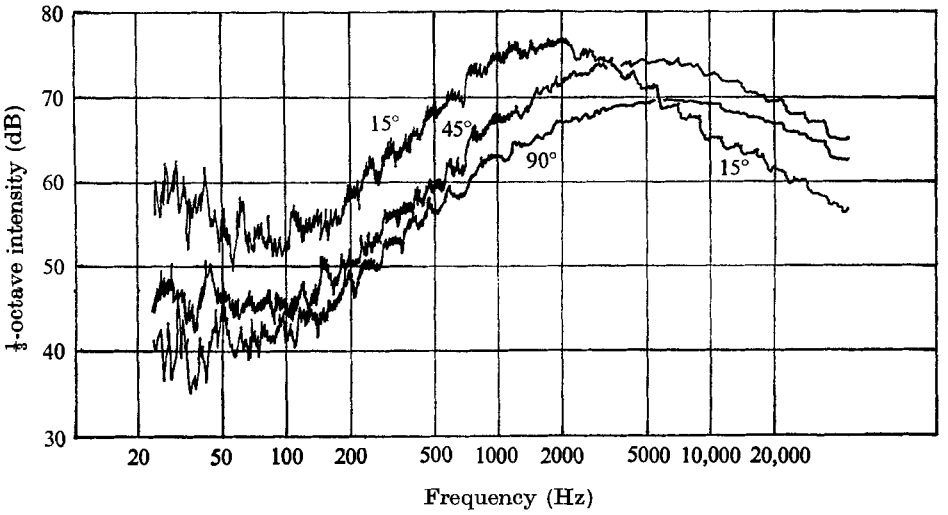

FIGURE 6. ⅓-octave spectra at 15°, 45° and 90° for jet velocity of 195 m/s.

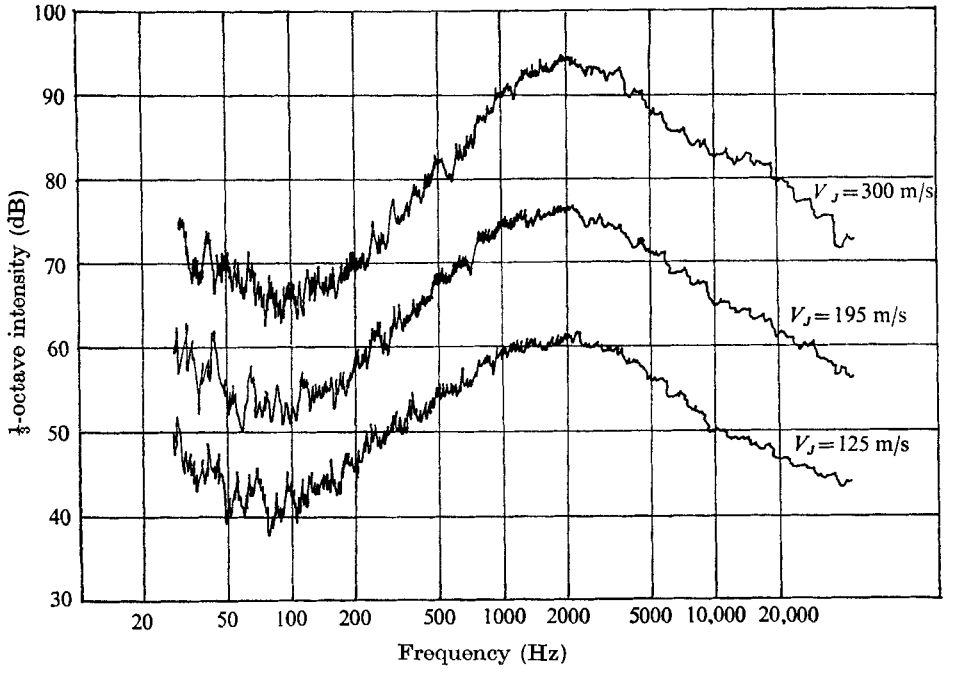

FIGURE 7. ⅓-octave spectra at 15° for various jet velocities.

arguments, but the decay at high frequencies is more rapid than expected, between 3 and 6 dB per octave.

At other angles to the jet axis, in between 15° and 45°, the spectrum behaves in the same way, with a sharp peak which does not scale very well as a Strouhal number. The peak moves progressively to higher frequencies as the emission angle is increased and at about 45° or so the broad shape characteristic of the spectrum at 90° reappears and the peak frequency again scales as a Strouhal number (figures 19, 20).

This observation is the main result of this paper and can be used to explain the discrepancies in theory and experiment which have already been noted in this section and which will be examined in more detail by studying the results in $\frac{1}{3}$-octave bands at particular frequencies.

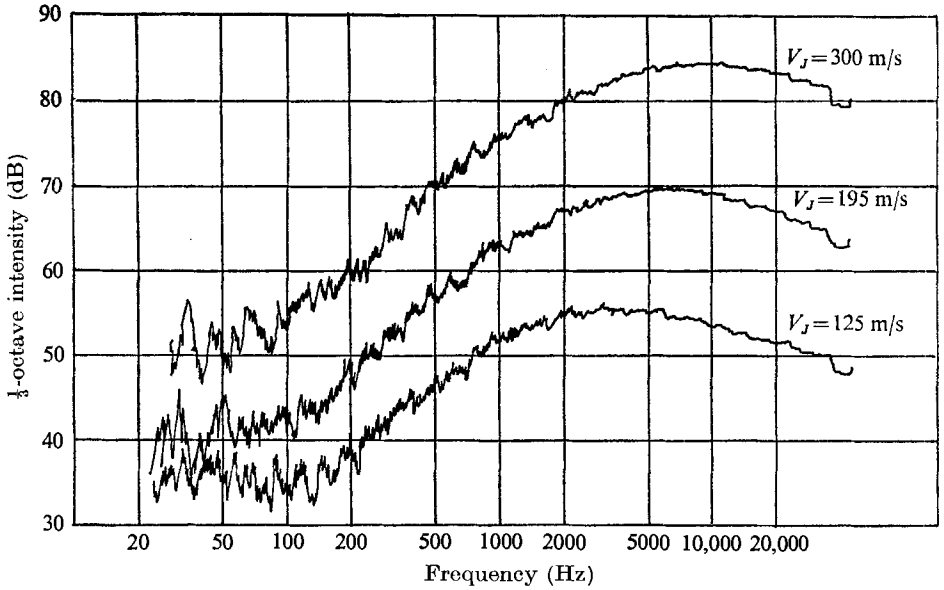

FIGURE 8. $\frac{1}{3}$-octave spectra at 90° for various jet velocities.

6. Analysis of results in $\frac{1}{3}$-octave bands

The results outlined above in §5 have been analysed in $\frac{1}{3}$-octave bands at particular values of the frequency parameter, $f_s D/V_J$, in accordance with the technique set out in §4. They are displayed both as velocity dependences and as directivities. There appears to be considerably more scatter in these results, especially at the lower jet velocities and at the lower frequencies. This is probably due to insufficient integration time at the lower frequencies, which leads to errors in reading the traces.

The dependence of $\frac{1}{3}$-octave intensities on jet velocity at three angles to the jet axis are shown in figures 9–11. Each figure has four values of the frequency parameter given by equation (9), namely 0·03, 0·1, 0·3 and 1·0. The theoretical predictions of equation (8) are also shown on these figures. The velocity dependence at 15° (figure 9) shows that the theory fits the results well at the two

lowest frequencies, i.e. $f_s D/V_J = 0{\cdot}03$ and $0{\cdot}10$. At the next value of the frequency parameter, 0·3, the theory is approximately in agreement at the low speeds but overestimates the intensity at the higher speeds. Similarly, the measurements at the highest frequency fall well below the expected variation.

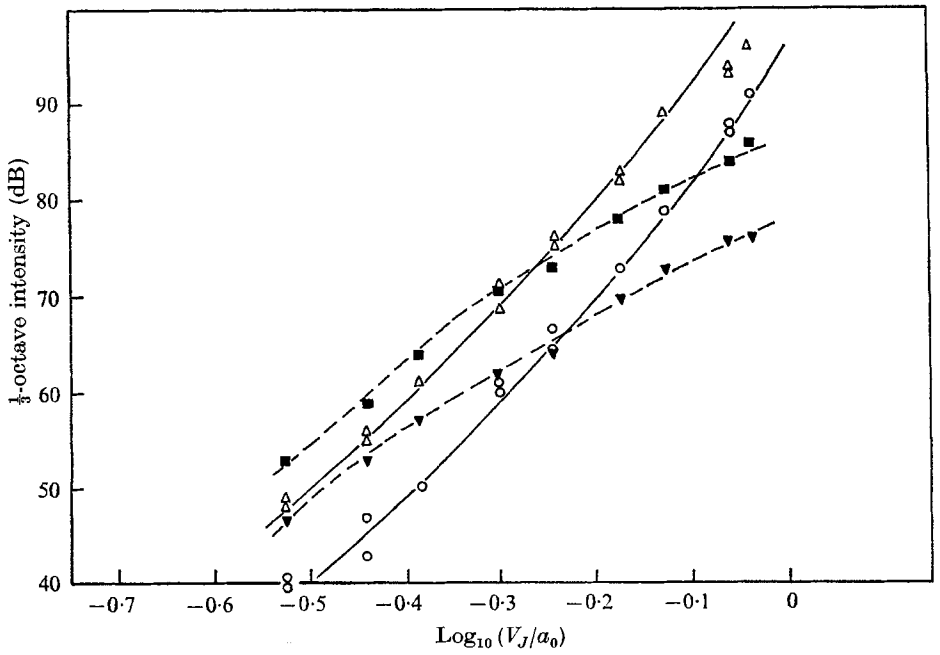

FIGURE 9. Velocity dependence of ⅓-octave intensity at 15° compared with theory. Values of $fD/V_J(1-M_c\cos\theta)$: ○, 0·03; △, 0·10; ■, 0·30; ▼, 1·0; ——, theory, equation (8).

The velocity dependence at 45° (figure 10) shows similar features except that the theoretically expected variation and the measurements also agree quite well at $f_s D/V_J = 0{\cdot}3$, but again the theory overestimates the intensity for $f_s D/V_J = 1{\cdot}0$, especially at the higher jet velocities. However, at 90° to the jet axis (figure 11), where convective effects are absent, the results follow the theoretical prediction, namely the eighth power of jet velocity, at all frequencies.

These results are also shown as directivities at three typical jet velocities in figures 12–14. The theoretical predictions of equation (8) for randomly oriented quadrupoles, i.e. with $D(\theta)$ equal to unity, are also shown and these have been adjusted vertically to give the best fit. At the lowest jet velocity (figure 12), the predicted directivity agrees fairly well with the measurements at all but the highest frequency. At the highest frequency the measurements fall below the prediction near the axis. Again, at the intermediate jet velocity (figure 13), the predicted directivity agrees well with the measurements for all but the highest frequency except near the axis, where the measurements are above the prediction. At the highest frequency the measurements fall well below the theoretical curve between the jet axis and 60° to the jet axis.

At the highest jet velocity (figure 14) the theoretical and measured directivities agree fairly well at the two lowest frequencies, except again the intensity is

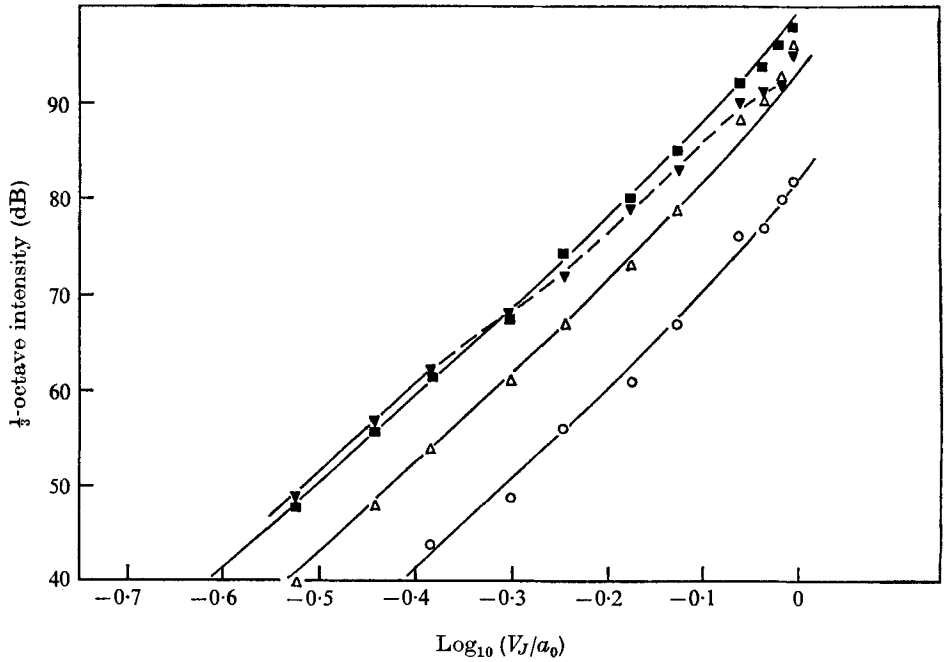

FIGURE 10. Velocity dependence of ⅓-octave intensity at 45° compared with theory. See figure 9 for symbols.

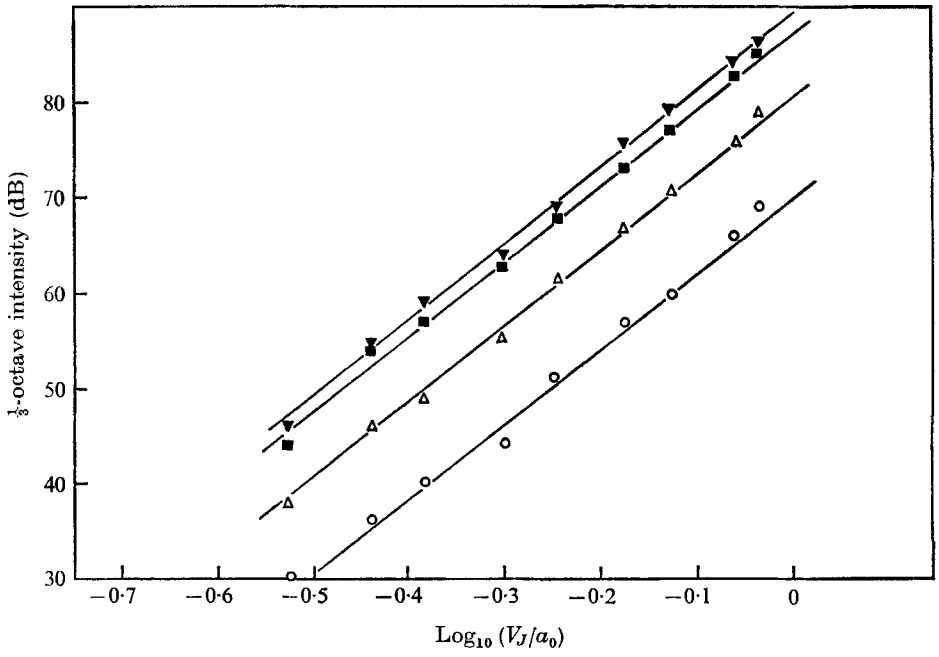

FIGURE 11. Velocity dependence of ⅓-octave intensity at 90° compared with theory. See figure 9 for symbols.

higher than predicted near the jet axis. At the two highest frequencies the measurements fall well below the prediction and at the highest frequency the measured directivity does not resemble the theoretical shape at all.

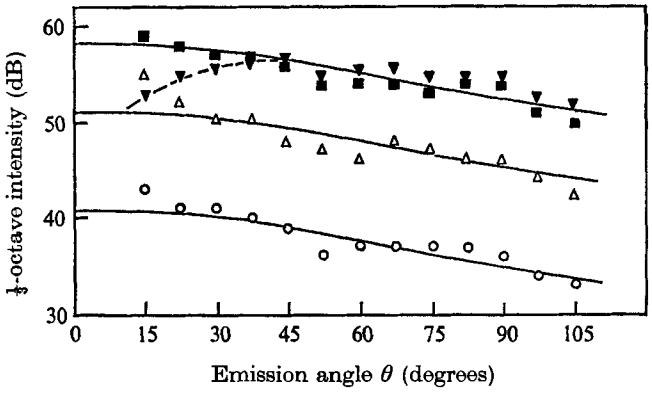

FIGURE 12. Directivity of ⅓-octave intensity for jet velocity of 125 m/s. Values of $fD/V_J(1-M_c\cos\theta)$: ○, 0·03; △, 0·10; ■, 0·30; ▼, 1·0; ——, theory, equation (8).

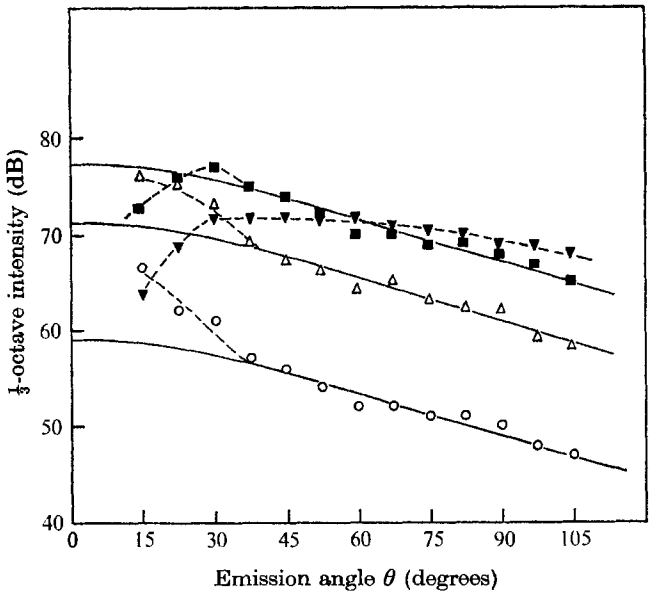

FIGURE 13. Directivity of ⅓-octave intensity for jet velocity of 195 m/s. See figure 12 for symbols.

To sum up, the analysis of the ⅓-octave intensities at various frequencies, f_sD/V_J, shows that the theoretical velocity dependence given by equation (8) fits the measured results at all angles to the jet axis for the lower frequencies. The directivity also given by (8) fits the results at angles away from the jet axis. Near the jet axis there is an unexpected increase in the measurements above the predicted directivity, although the velocity dependence at these angles is correctly predicted. The agreement is also good at the higher frequencies away

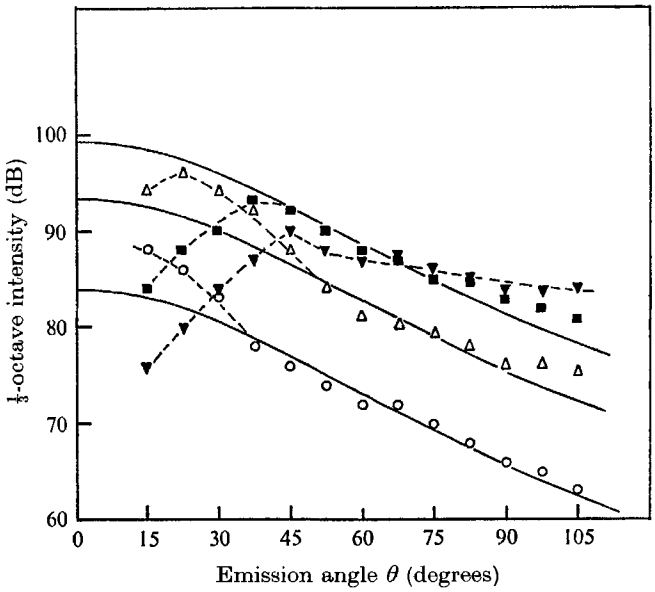

FIGURE 14. Directivity of ⅓-octave intensity for jet velocity of 300 m/s. See figure 12 for symbols.

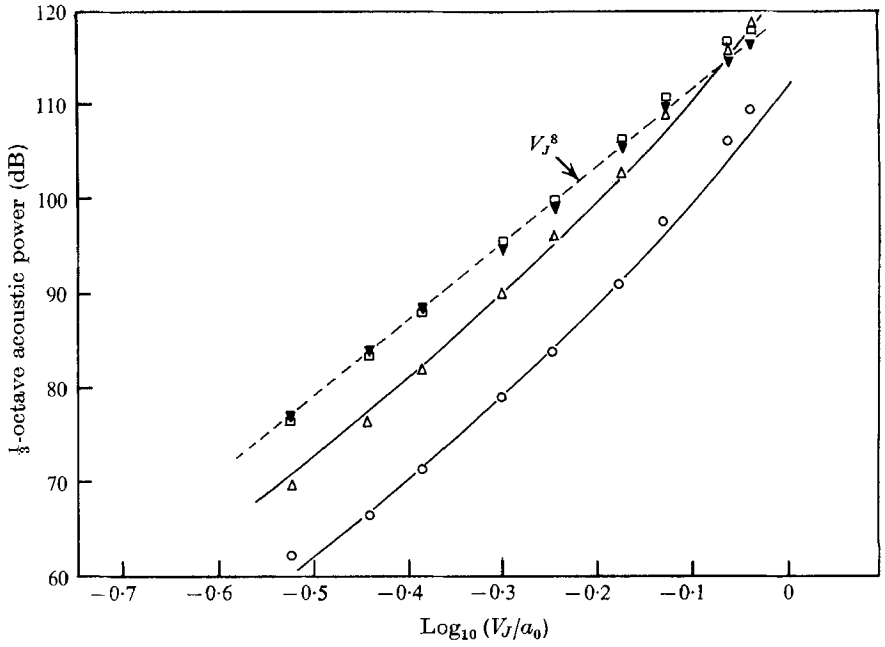

FIGURE 15. Velocity dependence of ⅓-octave acoustic power compared with theory. Values of $fD/V_J(1-M_c\cos\theta)$: ○, 0·03; △, 0·10; □, 0·30; ▼, 1·0; ——, theory, equation (11).

from the jet axis. However, at the high frequencies near the axis, the theory overestimates the measurements and, in particular, the velocity dependence falls below that expected.

The power in $\frac{1}{3}$-octave bands has also been calculated at the same values of the frequency parameter, $f_s D/V_J$. The velocity dependences of these results are shown in figure 15, along with the theoretical prediction of equation (11). It can be seen that, at the two lowest frequencies, the prediction agrees quite well with the measurements. However, at the highest frequencies the measurements do not show any convective amplification and are close to an eighth-power velocity dependence.

7. Discussion of the results

7.1. *Comparison of results with theory*

In general there is good agreement between the theoretical prediction and the measurements. For instance, the intensity at right angles to the jet varies as the eighth power of jet velocity, as indicated by the theory. However, it appears that the predicted amount of convective amplification, particularly near the jet axis, is not present. The analysis in $\frac{1}{3}$-octave bands at particular values of the frequency parameter, $f_s D/V_J$, shows that the correct amount of convective amplification is observed at the low frequencies, for $f_s D/V_J$ below about 0·1 (figures 9, 10). Again the theory fits well at all frequencies away from the jet axis (figure 11). However, at high frequencies for $f_s D/V_J$ above about 0·1 and near the jet axis, the measurements fall well below the theory (figure 9).

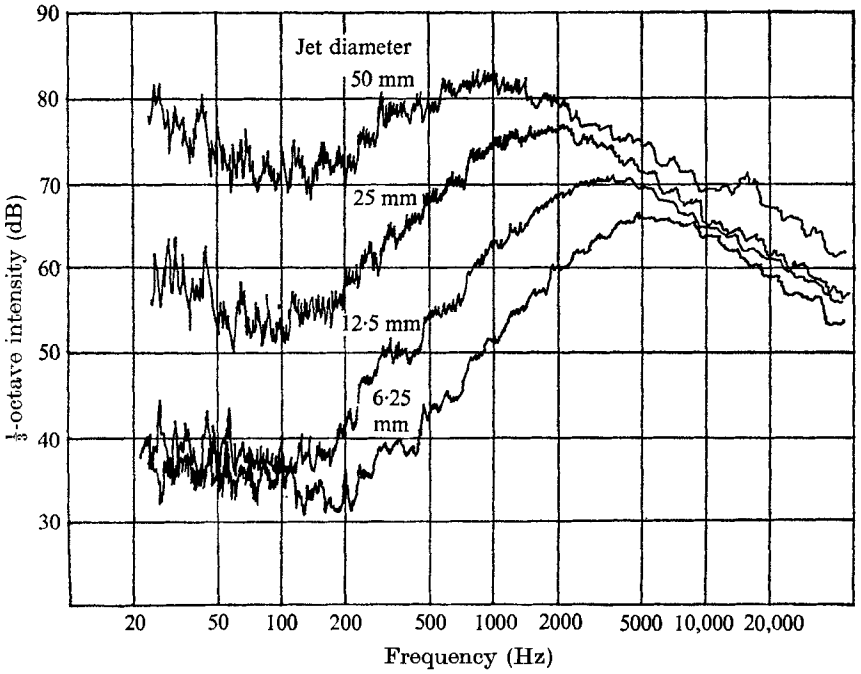

FIGURE 16. $\frac{1}{3}$-octave spectra at 15° for various nozzle diameters.

This discrepancy can be associated with the sharp decay of the spectrum from the peak at angles close to the axis (figure 7). The peak frequency of this spectrum appears to correspond to a critical frequency above which the theory and measurements disagree. It has already been noted in § 5 that this frequency is independent of jet velocity. Comparison with the corresponding spectra of the noise from 50, 12·5 and 6·25 mm nozzles shows that this frequency is also inversely proportional to jet diameter (figure 16). Examination of this frequency at various angles to the jet axis shows that it increases with angle until about 45° or so, the exact angle depending on the jet velocity, when it again scales on Strouhal number (figures 19, 20).

Another discrepancy between theory and measurement was also noticed in the directivity of $\frac{1}{3}$-octave intensity in the low frequencies and close to the jet axis. In the region of 15–30° the measurements are between 3 and 6 dB above the predicted amount for randomly oriented quadrupoles. Corresponding analyses for the 50 and 12·5 mm jets also show exactly the same discrepancy (figure 17). The appearance of this effect over the whole speed range and for several different nozzle sizes precludes the possibility that the microphone, when close to the jet axis, is recording strong near-field pressures from the fairly low frequency sources (figure 2).

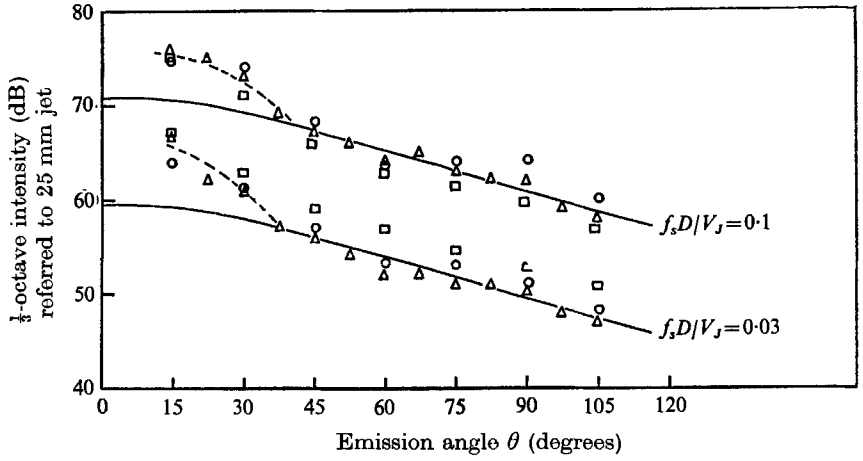

FIGURE 17. Directivity of $\frac{1}{3}$-octave intensity at low frequency at jet velocity 195 m/s compared with theory. Nozzle diameters: ○, 12·5 mm; △, 25 mm; □, 50 mm; ——, theory, equation (8).

Although a large ground reflexion from the supporting structure of the microphone stand was eliminated before these experiments were done, it is not possible to say that all reflexions from the microphone stand were removed. However, since this effect is noticed over a wide range of frequencies, it is reasonable to suppose that it is not due to an unwanted reflexion of the sound.

The measured velocity dependence near the axis shows the correct amount of convective amplification at these low frequencies, but, since the emission angle is fixed, any directivity other than that due to convection would not be observed until the directivity at these frequencies was studied. It is probable

that this difference from the directivity due to convection alone is caused by a preferred orientation of the quadrupoles. The difference in this case can be explained by a longitudinal quadrupole aligned along the jet axis, which has an unconvected directivity pattern given by $\cos^4\theta$. Since the intensity along the axis is increased by about 5 dB, it appears that the longitudinal quadrupole is approximately twice the strength of the randomly oriented quadrupole distribution at these frequencies. At higher frequencies it is not possible to speculate on the type of quadrupole present because the velocity dependences near the jet axis fall below the predicted curves, indicating that some other effect is present.

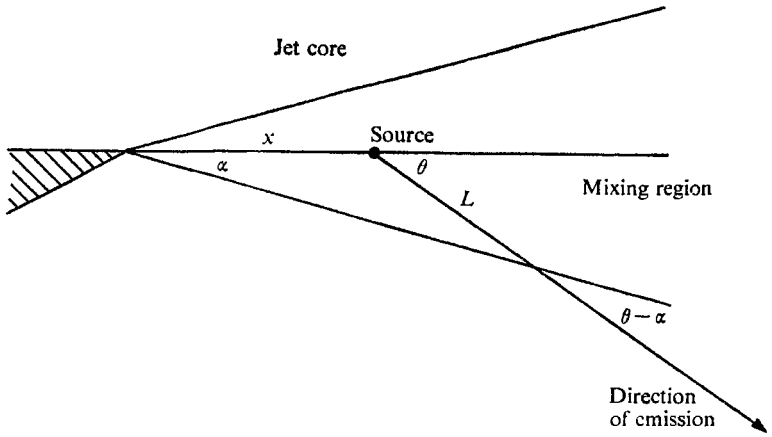

FIGURE 18. Diagram of mixing layer showing sound path length (L).

7.2. *Explanation of the critical frequency*

It has already been noted that the main disagreement between the theoretical prediction and experimental measurement occurs for the high-frequency sound at emission angles near the jet axis. This suggests that, whenever sound of shor wavelength is travelling through long stretches of the jet flow, the theoretical model fails. It seems likely that there is substantial interaction between the sound and the jet flow when the sound wavelength becomes shorter than the sound path length in the jet flow, but the exact nature of the interaction remains unknown. This idea may be quantified in a simple way by assuming that the sound sources are located downstream of the nozzle lip in the centre of the shear layer at a distance x, say. The shear layer is assumed to spread from the nozzle lip at a constant angle, α, to the jet axis. Therefore, the path length, L, in the turbulence zone is determined by the source position and the emission angle (figure 18).

A critical frequency, f_c, can be calculated on assuming

$$L = a_0/f_c, \tag{13}$$

where a_0 is the speed of sound in the external fluid and it is taken equal to the speed of sound in the turbulence region. The critical frequency is given by

$$f_c x/a_0 = \sin(\theta-\alpha)/\sin\alpha. \tag{14}$$

Since the radiated frequency is related to the source frequency by (5) and since the source frequency is approximately proportional to V_J/x, (14) reduces to a Mach number condition,

$$M_J = V_J/a_0 \sim [\sin(\theta-\alpha)/\sin\alpha](1-M_c\cos\theta). \tag{15}$$

However, if x is taken proportional to the jet diameter, D, (14) gives the dimensional variation of the critical frequency,

$$f_c D/a_0 \sim \sin(\theta-\alpha)/\sin\alpha. \tag{16}$$

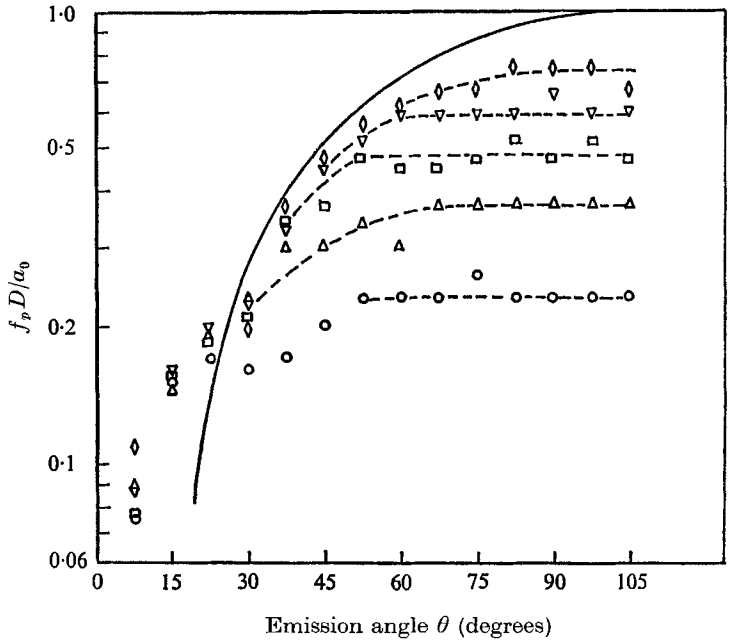

FIGURE 19. Variation of peak frequency, $f_p D/a_0$, with emission angle compared with theory. V_J/a_0: ○, 0·30; △, 0·41; □, 0·57; ▽, 0·75; ◇, 0·87; ——, theory, equation (16).

This expression may be compared with the measured variation of the critical frequency close to the jet axis. The peak frequencies, f_p, of spectra at various angles and jet velocities are shown as a function of emission angle in figure 19. At any particular jet velocity the peak frequency tends to be independent of emission angle away from the jet axis, but towards the jet axis the values fall on a locus which corresponds to the variation of critical frequency with angle. The theoretical locus given by (16), with $\alpha = 15°$ and constant of proportionality equal to 0·25, is also shown on figure 19.

It can be seen that there is some similarity between the measured locus and the variation of (16). At small angles to the jet axis, this simple model does not fit so well, possibly because the path length in the jet flow which effectively interacts with the sound is set more by the flow near the potential core rather than by the flow of the whole jet. For instance, at $7\frac{1}{2}°$ to the jet where the path length of the sound would be wholly in the flow, the critical frequency is about 1000 Hz for the 25 mm nozzle, indicating that the effective path length is about

10 diameters. At angles nearly at right angles to the jet axis, it might be erroneous to conclude that the peak frequencies at sufficiently high jet velocity would collapse on to the theoretical curve of critical frequency, since it seems likely that the peak frequency at right angles to the jet will continue to scale as a Strouhal number as the jet velocity is increased.

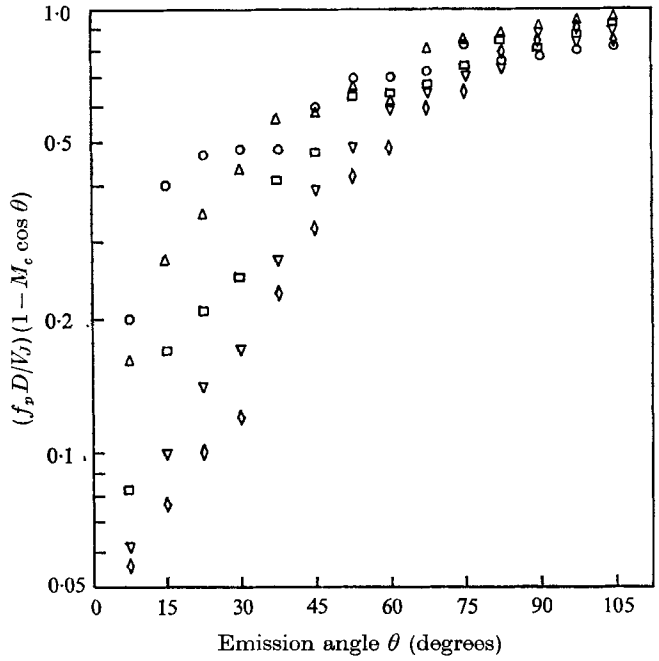

FIGURE 20. Variation of peak frequency $(f_p D/V_J)(1-M_c\cos\theta)$ with emission angle. See figure 19 for symbols.

7.3. *Effect of sound–jet flow interaction on the radiation*

The analysis in $\frac{1}{3}$-octave bands at various frequencies shows that there is sound energy missing compared with the theoretical predictions in the high frequencies and close to the jet axis (figures 9–14). It is expected that, if the sound is scattered or refracted by the flow after generation according to the convected quadrupole model, then the result of integrating the contributions at particular frequencies over all angles and the contributions at particular angles over all frequencies should capture the missing sound energy and confirm the theoretical prediction. It is assumed that the missing sound energy is not re-directed upstream or changed drastically in frequency where it would not be detected.

However, the analysis of the integrated sound energy (intensity, power in $\frac{1}{3}$-octave bands and overall power) shows that, compared with the theoretically expected result, there is still energy missing (figures 3, 5, 15). Because of this, it may be concluded that the scattering or refraction of the sound after it has been generated according to the convected quadrupole model does not occur to any great extent. Consequently, the interaction between the sound and the jet flow

interferes with the mechanism of sound generation and reduces the expected output in the high frequencies and close to the jet axis.

It can be seen from figure 9 that at 15° to the axis and in the high frequencies the velocity dependence of the $\frac{1}{3}$-octave intensity falls below the eighth power at the higher speeds. However, if these results are re-analysed without the Doppler correction and at a constant Strouhal number, the velocity dependence at the higher speeds is now near the eighth power (figure 21). It may be concluded then that, since the eighth power of velocity is still observed, the quadrupole source strength is unaffected and the effect of the interaction of the sound with the jet flow is to destroy, partially at any rate, the convective amplification for the high frequencies and close to the jet axis.

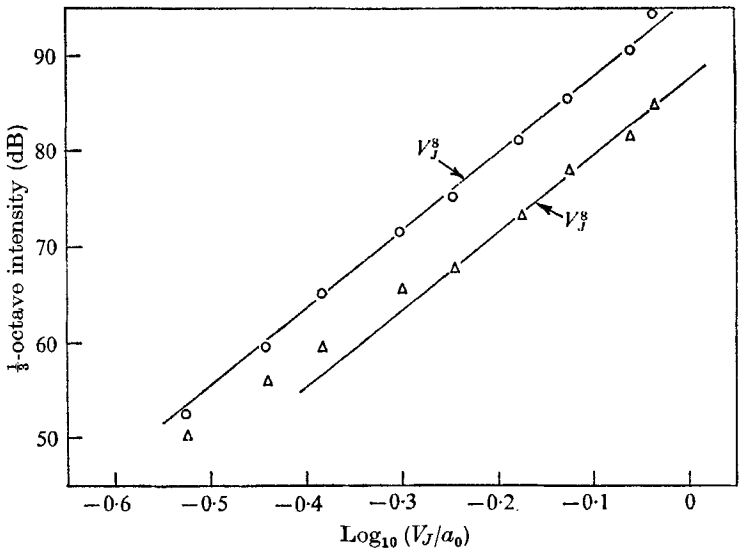

FIGURE 21. Velocity dependence of $\frac{1}{3}$-octave intensity at 15°.
Values of fD/V_J: ○, 0·3; △, 1·0.

The critical frequency, above which the convective amplification is largely destroyed, is dependent on jet diameter and the angle to the jet axis, and independent of the jet velocity, as discussed in §7.2. However, since the peak frequency of the spectrum unaffected by this phenomenon is dependent on jet velocity as well as diameter, and independent of angle, the difference between the peak frequency and the critical frequency at any angle is set by the Mach number V_J/a_0. It is found that for radiation close to the jet axis these two frequencies coincide when V_J/a_0 is approximately equal to 0·2. At angles further from the jet axis this critical Mach number is higher. Below a Mach number of about 0·2 the peak frequency is less than the critical frequency close to the jet axis and it would be expected that the intensity and power of the radiation would conform with the theoretical variations described in §4. Above this Mach number the peak frequency will be greater than the critical, and the convective amplification will be largely destroyed, as observed in the experimental results. Since the critical Mach number of 0·2 is very low when considering

jet noise generation, almost all jets will be affected by this sound–jet flow interaction to some extent and the effect will spread to larger emission angles as the jet velocity is increased.

8. Conclusions

Satisfactory measurements of the noise from a subsonic jet were achieved by employing suitable acoustic treatment and a large area contraction ratio to remove upstream noise sources. Unwanted near-field noise was avoided by placing the measuring point at 120 nozzle diameters from the jet. The measurements were restricted to a jet velocity range of 90–300 m/s by background noise at the lower speed and by the appearance of shock cell tones at the higher speed.

The acoustic efficiency of the jet noise was found to be $0{\cdot}8\text{–}1{\cdot}0 \times 10^{-4} M_J^5$, a value in close agreement with the experimental results of others (Lighthill 1963). The results showed that the acoustic power and intensities at all angles to the jet axis varied as the eighth power of jet velocity approximately. The peak frequencies of the $\frac{1}{3}$-octave spectra scaled on Strouhal number at emission angles at right angles to the jet. However, between 45° and the jet axis the peak frequencies showed poor scaling on Strouhal number but scaled better on fD/a_0.

A more detailed analysis of these results in $\frac{1}{3}$-octave bands was made at particular values of the frequency parameter, $(fD/V_J)(1 - M_c \cos\theta)$, which corrects the observed frequency so that the source in geometrically similar positions in the jet is analysed whatever the jet velocity, jet diameter and emission angle. These results show that Lighthill's theory of a convected distribution of quadrupoles fits the measurements well at low frequencies ($fD/a_0 < 0{\cdot}15$) for all emission angles. The analysis of the directivity also indicates that in addition to the randomly oriented quadrupole distribution, there is a longitudinal quadrupole present of approximately twice the strength of the randomly oriented quadrupole. The theory also fits well for higher frequencies as the emission angle approaches 90° to the jet axis. The theory overestimates the measurements for high frequencies ($fD/a_0 > 0{\cdot}15$) emitted close to the jet axis.

The discrepancy in the high frequency appears to be associated with a critical frequency above which the convective amplification is much reduced. This critical frequency is inversely proportional to jet diameter and increases with emission angle but it is independent of jet velocity. This suggests that the effect occurs when the wavelength of the radiated sound becomes shorter than the sound path length in the jet flow.

Since the peak frequency of the unaffected spectrum is proportional to V_J/D and the critical frequency to a_0/D, the resulting modification to the radiation will depend upon the Mach number, V_J/a_0. It is found that for the radiation close to the jet axis these two frequencies coincide at a Mach number of about 0·2, i.e. 60 m/s. Above this jet velocity the peak frequency of the noise is greater than the critical frequency and consequently the bulk of the noise is affected. The result is an apparent reduction in the convective amplification, so that the intensity, particularly at angles near the jet axis, and the acoustic power vary

at a power of jet velocity much nearer to the eighth than the higher power that would be expected from the theory.

The author is grateful to Prof. J. E. Ffowcs Williams, Prof. G. M. Lilley, Prof. P. E. Doak, Dr M. J. Fisher and Dr C. L. Morfey for their help and encouragement during the course of this work. The author is also grateful to Mr T. Grevle, who carried out the majority of the experiments, and to the National Gas Turbine Establishment, who provided financial assistance.

REFERENCES

DAVIES, P. O. A. L., FISHER, M. J. & BARRATT, M. J. 1963 The characteristics of the turbulence in the mixing region of a round jet. *J. Fluid Mech.* **15**, 337–367.

FFOWCS WILLIAMS, J. E. 1963 The noise from turbulence convected at high speed. *Phil. Trans. Roy. Soc.* A **255**, 469–503.

LIGHTHILL, M. J. 1952 On sound generated aerodynamically. 1. General theory. *Proc. Roy. Soc.* A **211**, 564–587.

LIGHTHILL, M. J. 1962 Sound generated aerodynamically. *Proc. Roy. Soc.* A **267**, 147–182.

LIGHTHILL, M. J. 1963 Jet noise. *A.I.A.A. J.* **1**, 1507–1517.